Characterization of the electronic properties of YB_{12}, ZrB_{12}, and LuB_{12} using ^{11}B NMR and first-principles calculations

2006 J. Phys.: Condens. Matter 18 2525

(http://iopscience.iop.org/0953-8984/18/8/015)

INSTITUTE OF PHYSICS PUBLISHING JOURNAL OF PHYSICS: CONDENSED MATTER

J. Phys.: Condens. Matter **18** (2006) 2525–2535 doi:10.1088/0953-8984/18/8/015

Characterization of the electronic properties of YB_{12}, ZrB_{12}, and LuB_{12} using ^{11}B NMR and first-principles calculations

B Jäger[1], S Paluch[2], O J Żogał[2], W Wolf[3], P Herzig[1], V B Filippov[4], N Shitsevalova[4] and Y Paderno[4,5]

[1] Institut für Physikalische Chemie, Universität Wien, Währinger Straße 42, 1090 Vienna, Austria
[2] Institute for Low Temperature and Structure Research, Polish Academy of Sciences, PO Box 1410, 50-950 Wrocław, Poland
[3] Materials Design s. a. r. l., 44, avenue F.-A. Bartholdi, 72000 Le Mans, France
[4] Institute for Problems of Materials Science, Academy of Sciences of Ukraine, 3 Krzhyzhanovsky street, 03680 Kiev, Ukraine

E-mail: peter.herzig@univie.ac.at

Received 16 August 2005
Published 10 February 2006
Online at stacks.iop.org/JPhysCM/18/2525

Abstract

Three metallic dodecaborides, YB_{12}, ZrB_{12} and LuB_{12}, have been investigated by electric-field gradient (EFG) measurements at the boron sites using the ^{11}B nuclear magnetic resonance (NMR) technique and by performing first-principles calculations. The NMR powder spectra reveal patterns typical for a completely asymmetric EFG tensor, i.e., an η parameter close to unity. The absolute values of V_{zz} (the largest component of the EFG) are determined from the spectra and they range between 11×10^{20} V m^{-2} and 11.6×10^{20} V m^{-2} with an uncertainty of 0.8×10^{20} V m^{-2}, being in very good agreement with the first-principles results. In addition the electronic structure and chemical bonding are analysed from partial densities of states and electron densities.

1. Introduction

Valence fluctuations, superconductivity and negative thermal expansion are some of the phenomena discovered in certain metal dodecaborides that raised considerable interest in this class of compounds [1]. The incomplete 4f shells of rare-earth constituents cause magnetic ordering at low temperature [2] or a mixed valence state in the case of YbB_{12} [3]. Superconductivity was reported in the diamagnetic dodecaborides ScB_{12}, YB_{12}, ZrB_{12} and LuB_{12} at the rather low temperatures of 0.39, 4.7, 5.82 and 0.4 K, respectively [4, 5]. Although recent studies [6] did not confirm the transition temperature of 4.7 K for YB_{12}, the temperature

[5] Deceased.

of about 6 K for ZrB_{12} has been validated [7]. The negative thermal expansion in YB_{12} and LuB_{12} was reported [6] and explained as a consequence of nearly non-interacting freely oscillating metal ions in cavities of a simple cubic rigid Debye lattice that is formed by B_{12} cage units.

The above electric, magnetic, and other bulk properties are determined by the electronic structure of these compounds in conjunction with their peculiar crystal structure. Most metal dodecaborides, MB_{12}, crystallize in the UB_{12} structure, in which the metal atoms and cuboctahedral B_{12} clusters are arranged as in the NaCl structure. In particular the favourable electric conductivity properties of the dodecaborides of trivalent metals are caused by the third valence electron which enters into the conduction band while the other two valence electrons are necessary for the formation of the B_{12} clusters [8–10]. For a better understanding of these properties, we have calculated the electronic structures of YB_{12}, ZrB_{12} and LuB_{12} (the latter including occupied $4f^{14}$ states) by methods based on density functional theory. Earlier calculations on YB_{12} and ZrB_{12} [11] were performed in order to discuss their superconducting properties in relation to those of the diborides MgB_2, YB_2, and ZrB_2, whereas for LuB_{12} only the total density of states was reported [12]. In the present study all the details of the electronic structure nowadays available from computational quantum physics, such as the position of the conduction band and the Fermi level, the partial local densities of states including crystal field split, and electron densities, are provided, which have not been reported so far.

In addition, electric-field gradients (EFGs) are considered. Using nuclear magnetic resonance (NMR) techniques they can be obtained for nuclei which possess a non-vanishing quadrupole moment and which are in an environment whose symmetry is lower than cubic. Comparison of these data from our ^{11}B NMR measurements with results from our first-principles calculations provides information on the validity of the assumed structure model and establishes a very reliable test of the calculated charge distribution, since the EFG is a local quantity sensitive to the environment of particular atoms in a crystal lattice. In addition, all EFG tensor components can be calculated, including their signs, whereas experimentally often only the component with the largest absolute value and the asymmetry parameter can be measured. Previously calculated EFGs in YB_4 and YB_6 [13] showed their very good agreement with experimental values. Moreover, they indicated that the main contribution to the EFG comes from the p–p sphere component. The lattice contribution is usually opposite in sign to the sphere contribution and is smaller in YB_4 than in YB_6.

In the UB_{12} structure (space group $Fm\overline{3}m$, no. 225) the metal atoms are in a cubic environment whereas the site symmetry of the boron atoms is C_{2v}. Therefore, only the EFG at the boron site can be measured using the ^{11}B nucleus which has a nuclear spin of $3/2$ and which implies a non-zero quadrupolar moment. For YB_{12}, ZrB_{12}, and LuB_{12} the B–B distances between neighbouring cuboctahedra are slightly shorter than within the cuboctahedron (for YB_{12}: 1.72 Å compared to 1.79 Å; the corresponding values for ZrB_{12} are 1.68 and 1.78 Å, and for LuB_{12} 1.70 and 1.79 Å, respectively).

2. Structural parameters

For YB_{12}, ZrB_{12} and LuB_{12} all structural parameters have been optimized using the Vienna *ab initio* simulation package (VASP) [14–16]. By this method the Kohn–Sham equations of density-functional theory [17, 18] with periodic boundary conditions are solved within a plane-wave basis set with electron–ion interactions described by the projector augmented wave (PAW) method [19, 20]. Exchange and correlation are treated within the generalized-gradient approximation (GGA) [21]. The structural parameters were calculated by atomic forces and stress-tensor minimization. For the plane-wave basis a cutoff energy of 400 eV has been used.

Table 1. Structural parameters used in the EFG and electronic-structure calculations for the dodecaborides with UB_{12} structure ($Fm\bar{3}m$, no. 225). (Note: The lattice parameters are in Å, and the positional parameter refers to site 48i of B).

Compound	Lattice parameter a	Positional parameter x	Remarks
YB_{12}	7.4995	0.668 90	Calculated, VASP (GGA)
	7.500	0.670 6	Experimental, [22]
ZrB_{12}	7.4085	0.669 62	Calculated, VASP (GGA)
	7.4043	0.669 82	Experimental, [23]
LuB_{12}	7.4549	0.669 14	Calculated, VASP (GGA)
	7.4710	0.669 4	Experimental, [24]

The calculated structural parameters are compared to experimental data in table 1, demonstrating very good agreement. For the calculation of the EFGs (section 3) and for the analysis of the electronic structure and chemical bonding (section 4) the structural parameters from the recent measurements have been used for ZrB_{12} and LuB_{12}, as given in table 1. For YB_{12}, experimental data are much less recent. Consequently, for YB_{12} the calculated lattice parameters have been used in all further investigations.

3. Electric-field gradients

3.1. Experimental details

To avoid skin-depth effects for better RF penetration, the samples were used in powder form and obtained by crushing the compact synthesized polycrystalline samples ($Y_{0.92}B_{12}$, LuB_{12}) or single crystals (ZrB_{12}, $LuB_{11.9}$). The different preparational procedures of the source substances are connected with the conditions of obtaining single-phase powders which depend on the phase diagrams of these compounds [25]. In the case of yttrium dodecaboride it is easier to obtain the single-phase synthesized powder by borothermal reduction of yttrium oxide with a boron-rich composition. For zirconium dodecaboride, on the other hand, single-crystal growing by inductive zone melting from a mixture of zirconium di- and dodecaborides is the only possibility for obtaining the single-phase product [26]. Lutetium dodecaboride was obtained in slightly different compositions by the two preparational methods. However, it became immediately obvious that the NMR signals were very similar for both samples. The studied samples were highly pure due to the high purity of the source oxides (4–5 N) and the amorphous boron (3 N). The process of synthesis and zone melting resulted in additional purification from highly volatile impurities in the boron used as starting material.

The NMR measurements were carried out with a Bruker DSX300 spectrometer in a magnetic field of 7.05 T. The ^{11}B spectra were obtained by Fourier transformation of the second half of the quadrupolar echo signal following two 1 μs pulses. The spectra contain up to 256 accumulations with a repetition time of 20 s and a dwell time of 0.1 μs.

3.2. First-principles calculations

The all-electron band-structure calculations for the calculation of EFGs are based on density-functional theory (DFT) [17, 18] and the local-density approximation and have been performed by the linearized augmented plane-wave (LAPW) method [27] in its full-potential version [28–31] (FLAPW) using an exchange–correlation potential by Hedin and Lundqvist [32, 33].

The following parameters have been used in the FLAPW calculation. For the l expansion of the potential and the electron density inside the muffin-tin spheres, terms up to $l = 8$ were taken into account. The muffin-tin radii were chosen as $R_Y = 1.3759$ Å and $R_B = 0.8567$ Å for YB_{12}, $R_{Zr} = 1.4817$ Å and $R_B = 0.7805$ Å for ZrB_{12}, and $R_{Lu} = 1.5875$ Å and $R_B = 0.7805$ Å for LuB_{12}. Plane waves for the wave functions in the interstitial were included for **k** vectors up to a length of about 4.3 (in units of $2\pi/a$), which corresponds to roughly 930 basis functions per formula unit. In the SCF procedure for the valence states a $15 \times 15 \times 15$ Monkhorst and Pack mesh was adopted which is equivalent to 120 **k** points. The higher-lying metal core states (4s for YB_{12}, 4s and 4p for ZrB_{12}, and 5s and 5p for LuB_{12}) have been treated as band states in a second energy window using an $11 \times 11 \times 11$ Monkhorst and Pack mesh (56 **k** points), while the 4p states of YB_{12} were calculated in the energy window of the valence states. The reciprocal-space integration has been performed by using the linear tetrahedron method [34, 35]. The calculations are set up to ensure a high level of convergence with respect to all computational parameters, making the approximations inherent in density functional theory the main source of possible errors.

The EFGs have been calculated from the $l = 2$ components of the Coulomb potential near the nuclei. The formalism by Herzig [36] and Blaha *et al* [37] has also been employed to split the calculated EFG components into the contributions from the surrounding electrons within the respective muffin-tin sphere ('sphere contribution') and the remainder that comes from outside this sphere ('lattice contribution'). This partitioning depends, to a small extent, on the choice of the muffin-tin radii. The valence contribution can be split further into the allowed ll' contributions (only sd, pp, pf are important in the present context) which provide useful information about the influence of particular l-like wavefunctions on the EFGs [38]. As is common practice the EFG tensor is transformed to principal axes and the resulting EFG component with the largest absolute value is always designated as V_{zz}.

3.3. EFGs: results and discussion

Figure 1 shows the ^{11}B spectrum for YB_{12} which is typical for a nuclear spin $I = 3/2$ in the presence of first-order quadrupole effects. Contrary to the situation in the YB_4 and YB_6 spectra [13] where sharp maxima of satellites (due to $3/2 \leftrightarrow 1/2$ and $-3/2 \leftrightarrow -1/2$ transitions) are observed, for YB_{12} only the satellite steps at $\nu_Q = 3\,e^2qQ/2I(2I-1)h$ are visible on the frequency scale. Here, eq is the modulus of the largest component of the EFG tensor, eQ is the nuclear electric quadrupole moment, I is the nuclear spin, and h is Planck's constant. The different behaviour is due to the fact that in YB_{12} the EFG tensor is lacking axial symmetry. In this case when the asymmetry parameter $\eta = (V_{xx} - V_{yy})/V_{zz}$ is close to 1, the satellite maxima (singularities) move inside the central $(1/2 \leftrightarrow -1/2)$ transition and become unobservable. In such a situation the best way to estimate V_{zz} and η is the use of a simulation spectrum. For this purpose the DMFIT program [39] has been used. The results for YB_{12} and the two other investigated dodecaborides, ZrB_{12} and LuB_{12}, are shown in table 2.

For the dodecaborides with cuboctahedral B_{12} units the B atoms occupy sites of C_{2v} symmetry which leads to two independent EFG components and a non-zero asymmetry parameter η. In comparing the calculated and measured EFGs one notices that the experimental $|V_{zz}|$ values are systematically smaller than the calculated ones. Most probably this is due to a slightly too high ^{11}B nuclear quadrupole moment [40] used in the comparison. A similar behaviour has been found in our previous investigation on YB_4 and YB_6 [13]. Apart from this discrepancy the agreement is excellent—even the correct order of the very similar $|V_{zz}|$ values is correctly reproduced.

The principal axis for the most negative EFG component is determined by the strongest bonding interactions. For YB_{12} and LuB_{12} this is the V_{yy} component and for ZrB_{12}

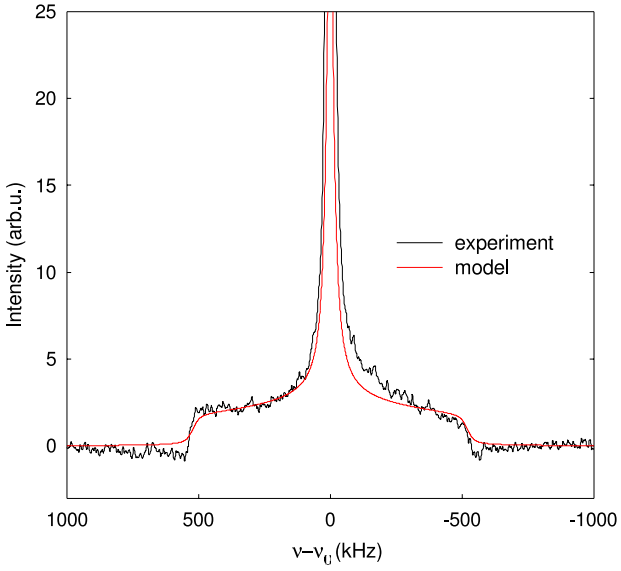

Figure 1. Experimental and theoretical (model) powder-pattern ^{11}B spectrum for YB_{12}. The steps at $|\nu - \nu_0| \approx 500$ kHz are noticeable.

(This figure is in colour only in the electronic version)

Table 2. Calculated B EFGs (in 10^{20} V m^{-2}) for YB_{12}, ZrB_{12}, and LuB_{12} compared to the experimental results assuming an ^{11}B nuclear quadrupole moment of 0.04 $|e| \times 10^{-28}$ m^2 [40]. (Note: The principal axes refer to the B atom at $\frac{1}{2}, x - \frac{1}{2}, x - \frac{1}{2}$.).

		Calculated			Experimental	
Compound	i	V_{ii}	η	Principal axes	$\lvert V_{ii}\rvert$	η
YB_{12}	x	−0.43		(1 0 0)		
	y	−11.83		$(0\ \frac{1}{\sqrt{2}}\ \frac{1}{\sqrt{2}})$		
	z	12.26	0.93	$(0\ \frac{1}{\sqrt{2}}\ -\frac{1}{\sqrt{2}})$	11.0 ± 0.8	0.93
ZrB_{12}	x	0.13		(1 0 0)		
	y	12.31		$(0\ \frac{1}{\sqrt{2}}\ -\frac{1}{\sqrt{2}})$		
	z	−12.38	0.98	$(0\ \frac{1}{\sqrt{2}}\ \frac{1}{\sqrt{2}})$	11.2 ± 0.8	0.94
LuB_{12}	x	−0.22		(1 0 0)		
	y	−12.55		$(0\ \frac{1}{\sqrt{2}}\ \frac{1}{\sqrt{2}})$		
	z	12.78	0.97	$(0\ \frac{1}{\sqrt{2}}\ -\frac{1}{\sqrt{2}})$	11.6 ± 0.8	0.98

the V_{zz} component. The corresponding principal axes are determined by the strongest bonding interactions which, in all three cases, is the inter-cuboctahedral B–B bond between neighbouring B_{12} units. An EFG calculation for B_{12} (same structure as for YB_{12} but with Y atoms removed) shows that the orientation of the principal axes is solely determined by the B atoms.

Now the split of the B EFGs into the lattice and sphere contributions and the latter into their main components (sd, pp, and pf) are considered (table 3). The sphere contribution is the one with the largest absolute value and the lattice contribution is much smaller but not

Table 3. Split of the B EFGs for YB_{12}, ZrB_{12}, and LuB_{12} into lattice and sphere components and the latter into their main contributions, i.e., sd, pp, and pf. All V_{zz} values are in units of 10^{20} V m^{-2}.

Compound	V_{zz}	V_{zz}^{lat}	V_{zz}^{sph}	V_{zz}^{sd}	V_{zz}^{pp}	V_{zz}^{pf}
YB_{12}	12.3	−1.8	14.0	1.0	12.0	0.7
ZrB_{12}	−12.4	2.0	−14.4	−0.8	−12.8	−0.7
LuB_{12}	12.8	1.3	14.1	0.8	12.4	0.6

negligible. As expected the pp component dominates the sphere contribution with the sd and pf components being the most important other components.

4. Electronic structure and chemical bonding

The first theoretical investigation of metal dodecaborides using a simple LCAO-MO approach was performed in 1963 by Lipscomb and Britton [10] in a fashion similar to the one by Longuet-Higgins and Roberts [8] for the metal hexaborides. According to these authors the cuboctahedral arrangement of the B atoms leads to six different bonding states which can accommodate 26 electrons (taking into account degeneracy). Since three valence electrons are provided by each B atom there are altogether 36 valence electrons coming from one B_{12} unit, of which twelve are required for the bonds each B atom forms with a B atom of a neighbouring B_{12} unit. Therefore the remaining 24 electrons plus two additional metal valence electrons are required to fill up all bonding orbitals of the cuboctahedral cluster, leaving one metal electron to occupy the conduction band which means that the dodecaborides are metals. Electronic-structure calculations by first-principles methods have been performed by Harima *et al* for YB_{12} [12] and LuB_{12} [12, 41] using the self-consistent APW method (band structures only). LuB_{12} has also been investigated by Heinecke *et al* [42] employing the WIEN version of the FLAPW method. These authors give the band structure, density of states (DOS), and the Fermi surface. Shein *et al* studied the electronic properties of YB_{12} [43] and ZrB_{12} [43, 11] using the FLMTO method. The latter authors do not show the lowest valence band corresponding to the totally symmetric state (a_{1g} of group O_h) of the cuboctahedral cluster and erroneously use the term 'icosahedral' instead of 'cuboctahedral' throughout their papers. In figure 2 the band structures for YB_{12}, ZrB_{12}, and LuB_{12} of the present work are presented.

The DOS curves for the three dodecaborides are given in figures 3–5 together with the local partial DOS components and the e_g/t_{2g} splitting for the metal d states. Apart from one additional valence electron for ZrB_{12} leading to a corresponding shift of the DOS curve in a rigid-band-like manner and the appearance of the Lu f states in the energy region of the valence electrons for LuB_{12}, the DOS curves are very similar for the three compounds. At energies of about −15 eV, B s character is predominant with a non-negligible B p component. In this energy range totally symmetric and therefore nodeless crystal orbitals form strong σ bonds between the boron atoms within the dodecahedral B_{12} units. They are clearly visible from the corresponding electron densities shown in figure 6.

After an energy gap of about 1.5 eV the boron DOS is first dominated by s character, then between about −10 and −7.5 eV s and p contributions are almost identical and at higher energies the ratio between s and p character decreases steadily. The metal DOS is very small below about −13 eV. Going to higher energies there is a repeated change between e_g and t_{2g} dominance until the Fermi level is reached. The metal e_g orbitals point towards the centres of the square faces of the B cuboctahedron and the t_{2g} orbitals towards the centres of the inter-cuboctahedral bonds.

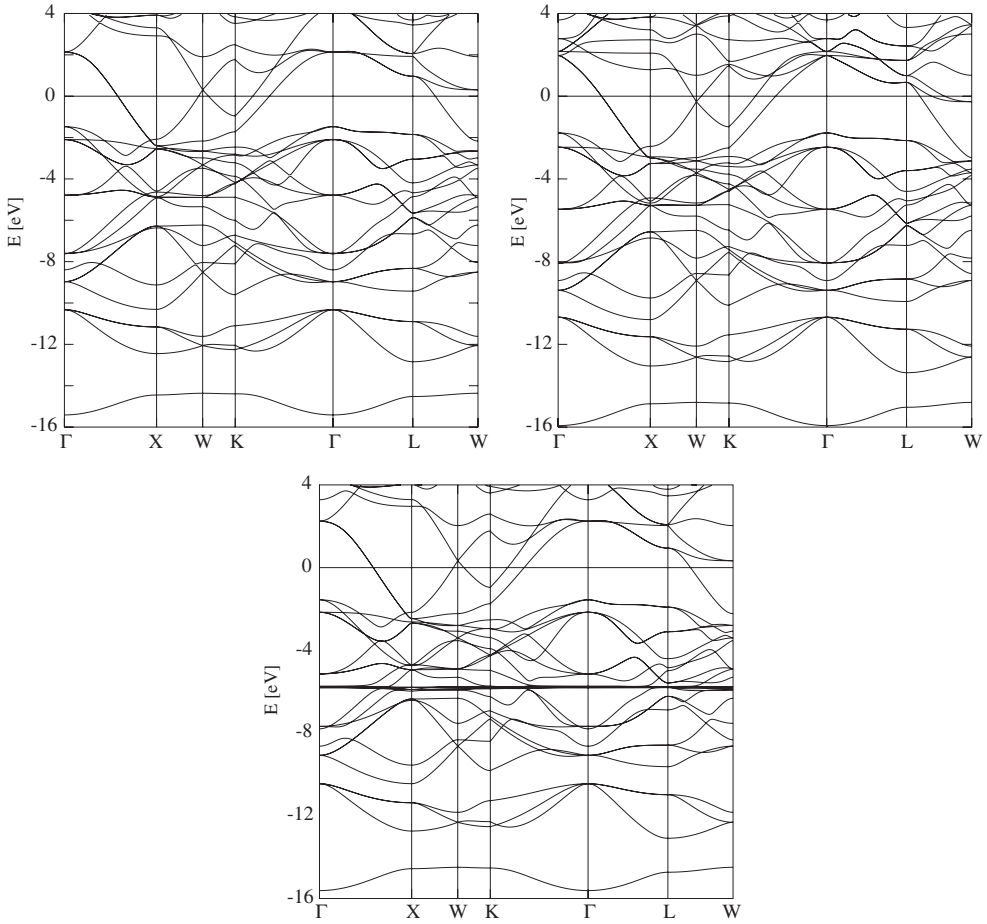

Figure 2. Electronic band structures for YB_{12} (top left), ZrB_{12} (top right), and LuB_{12} (bottom).

The bonding situation between the B atoms of neighbouring B_{12} cuboctahedra is dependent on the energy in a very systematic way. This has been studied by inspecting electron-density plots for a number of selected characteristic electronic states. At energies below roughly -10 eV, considerable bonding effects occur within the cuboctahedra. Above this energy, up to about -7 eV, σ bonds and between about -7 eV and the Fermi level mainly π bonds between adjacent B_{12} clusters are found. These states are, of course, also involved in bonding between B atoms of the same B_{12} unit and with e_g or t_{2g} states of neighbouring metal atoms.

The valence electron densities in the (001) plane through the metal atoms (see figure 7) show spherical densities for YB_{12} and LuB_{12}, while in ZrB_{12} the t_{2g} character prevails slightly due to the additional valence electron for this compound. Figure 7 also shows the strong covalent bonds between neighbouring boron cuboctahedra. Apart from the differences for the metal atoms the three valence electron densities are very similar.

In figure 8 the valence electron densities in the (001) plane through the B atoms in the three dodecaborides are displayed. There are two noticeable differences between the three dodecaborides. First, the electron density between the edges of neighbouring B_{12} cuboctahedra is slightly lower for YB_{12}, because this boride has the largest unit-cell volume of the three

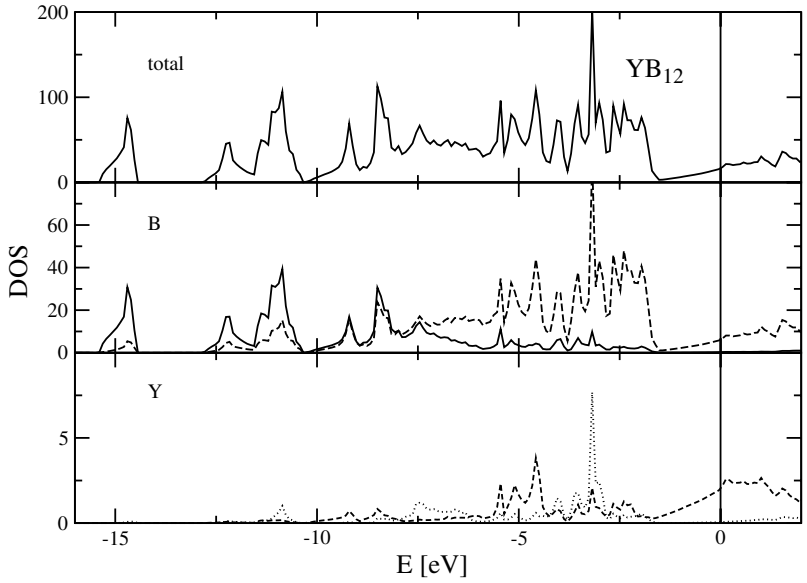

Figure 3. Total DOS (top) and local partial DOS components for YB_{12} (centre: B s, full line; B p, dashed line; bottom: Y e_g, dotted line; Y t_{2g}, dashed line) in units of states per Rydberg and per formula unit.

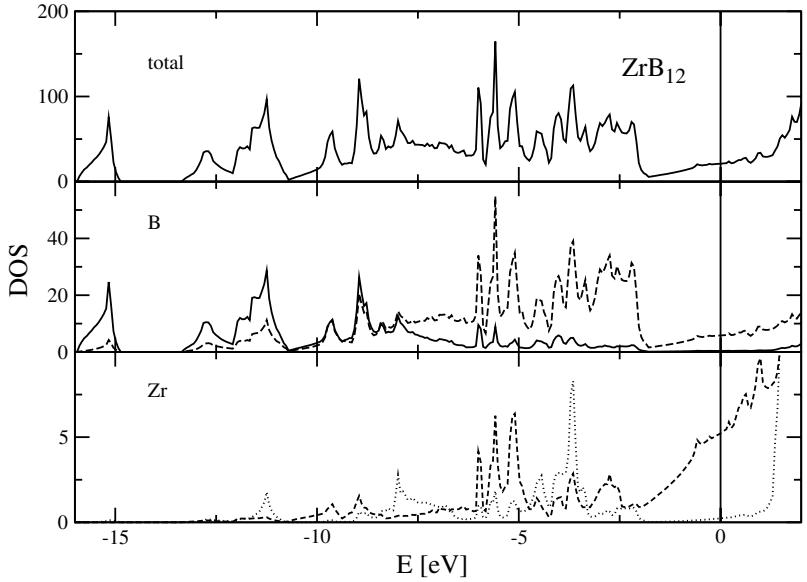

Figure 4. Total DOS (top) and local partial DOS components for ZrB_{12} (centre: B s, full line; B p, dashed line; bottom: Zr e_g, dotted line; Zr t_{2g}, dashed line) in units of states per Rydberg and per formula unit.

compounds and the dimensions of the B_{12} clusters are almost independent of the lattice parameters of the dodecaborides. Second, the electron densities in the (001) plane through

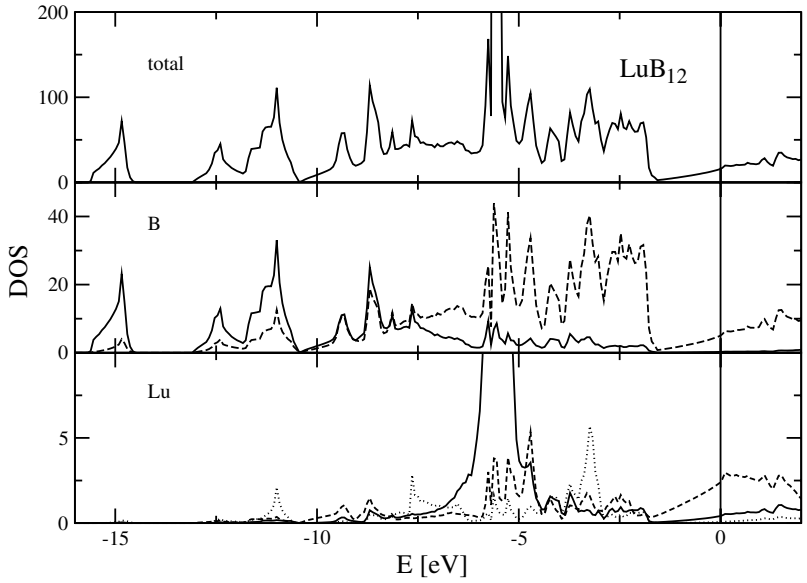

Figure 5. Total DOS (top) and local partial DOS components for LuB_{12} (centre: B s, full line; B p, dashed line; bottom: Lu e_g, dotted line; Lu t_{2g}, dashed line; Lu f, full line) in units of states per Rydberg and per formula unit.

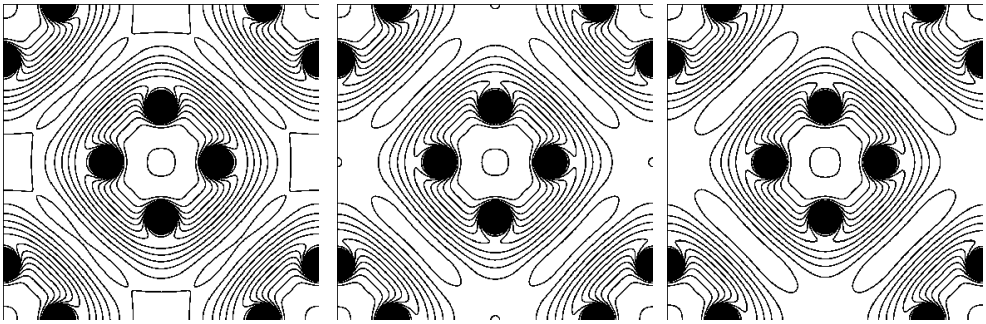

Figure 6. Electron densities in the (001) plane through the B atoms for the lowest valence bands at about -15 eV. Left: YB_{12}, centre: ZrB_{12}, right: LuB_{12}. A logarithmic grid of contour lines has been used ($x_i = x_0\, 2^{i/3}$).

the B atoms at the points above the metal atoms are highest for ZrB_{12} and lowest for YB_{12}. These points are found at the edge-centres of the corresponding density plots.

5. Summary

For YB_{12}, ZrB_{12}, and LuB_{12} we have performed electric-field gradient measurements at the B sites and also first-principles calculations in order to analyse the chemical bonding properties of these compounds and to compare the results of accurate experimental and computational methods. For the EFG very good agreement has been obtained. The calculations show that for the EFG the orientation of the principal axes is completely determined by the skeleton of the boron atoms and that the contribution of the B p electrons is the largest one.

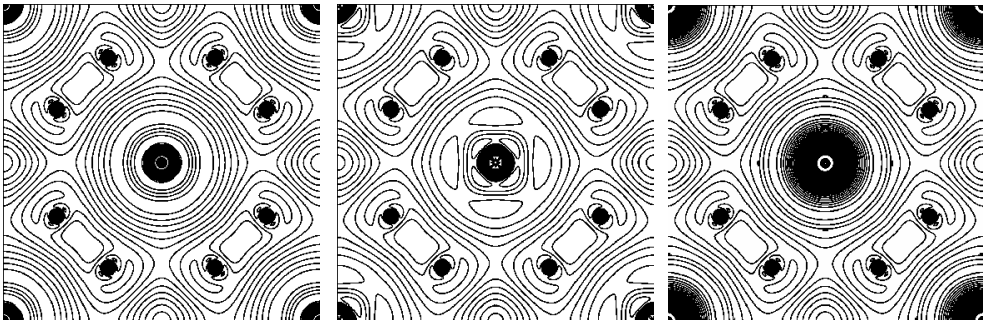

Figure 7. Valence electron densities in the (001) plane through the metal atoms. Left: YB_{12}, centre: ZrB_{12}, right: LuB_{12}. The metal atoms are situated in the centres and corners of the respective plots. A logarithmic grid of contour lines has been used ($x_i = x_0\, 2^{i/3}$).

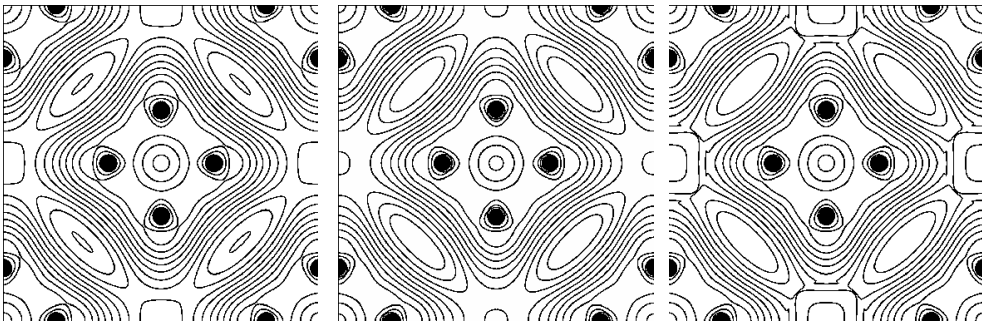

Figure 8. Valence electron densities in the (001) plane through the B atoms. Left: YB_{12}, centre: ZrB_{12}, right: LuB_{12}. A logarithmic grid of contour lines has been used ($x_i = x_0\, 2^{i/3}$).

As regards the electronic structure and chemical bonding, electron density plots show rather small differences between the three dodecaborides, although there are some variations in bonding between the B atoms belonging to adjacent B_{12} cuboctahedra. The importance of the low-lying valence band related to the totally symmetric molecular orbital for the cuboctahedral B_{12} units is stressed.

Acknowledgments

The authors would like to thank the Austrian Science Foundation (project no. P15801-N02) and INTAS (project 03-51-3036) for financial support. The calculations were performed on the Schrödinger II Linux cluster of the Vienna University Computer Centre.

References

[1] Etourneau J and Hagenmuller P 1985 *Phil. Mag.* B **52** 589–610
[2] Czopnik A, Shitsevalova N, Krivchikov A, Pluzhnikov V, Paderno Yu and Ōnuki Y 2004 *J. Solid State Chem.* **177** 507–14
[3] Kasaya M, Iga F, Takigawa M and Kasuya T 1985 *J. Magn. Magn. Mater.* **47–48** 429–35
[4] Matthias S T, Geballe T H, Andres K, Corenzwit E, Hull G W and Maita J P 1968 *Science* **159** 530
[5] Bat'ko I, Bat'ková M, Flachbart K, Filippov V B, Paderno Yu B, Shitsevalova N Yu and Wagner Th 1995 *J. Alloys Compounds* **217** L1–3

[6] Czopnik A, Shitsevalova N, Pluzhnikov V, Krivchikov A, Paderno Yu and Onuki Y 2005 *J. Phys.: Condens. Matter* **17** 5971–85
[7] Lortz R, Wang Y, Abe S, Meingast C, Paderno Yu B, Filippov V and Junod A 2005 *Phys. Rev.* B **72** 024547
[8] Longuet-Higgins H C and Roberts M de V 1954 *Proc. R. Soc.* **224** 336–47
[9] Johnson R W and Daane A H 1963 *J. Chem. Phys.* **38** 425–32
[10] Liscomb W N and Britton D 1960 *J. Chem. Phys.* **33** 275–80
[11] Shein I R and Ivanovskiĭ A L 2003 *Phys. Solid State* **45** 1429–34
Shein I R and Ivanovskiĭ A L 2003 *Fiz. Tverd. Tela* **45** 1363–8
[12] Harima H, Yanase A and Kasuya T 1985 *J. Magn. Magn. Mater.* **47/48** 567–9
[13] Jäger B, Paluch S, Wolf W, Herzig P, Żogał O J, Shitsevalova N and Paderno Y 2004 *J. Alloys Compounds* **383** 232–8
[14] http://cms.mpi.univie.ac.at/vasp/
http://www.materialsdesign.com/Pages/VASP.htm
[15] Kresse G and Furthmüller J 1996 *Phys. Rev.* B **54** 11169–86
[16] Kresse G and Furthmüller J 1996 *Comput. Mater. Sci.* **6** 15–50
[17] Hohenberg P and Kohn W 1964 *Phys. Rev.* B **136** 864–71
[18] Kohn W and Sham L J 1965 *Phys. Rev.* A **140** 1133–8
[19] Blöchl P E 1994 *Phys. Rev.* B **50** 17953–79
[20] Kresse G and Joubert D 1998 *Phys. Rev.* B **59** 1758–75
[21] Perdew J P, Chevary J A, Vosko S H, Jackson K A, Pederson M R, Singh D J and Fiolhais C 1992 *Phys. Rev.* B **46** 6671–87
[22] Matkovic V I, Economy J, Giese R F Jr and Barrett R 1965 *Acta Crystallogr.* **19** 1056–8
[23] Leithe-Jasper A, Sato A and Tanaka T 2002 *Z. Kristallogr. NCS* **217** 319–20
[24] Pietraszko A, Czopnik A, Shitsevalova N and Paderno Y 2000 *19th European Crystallographic Mtg (Nancy, France, August 2000)*
[25] Massalski T B 1996 *Binary Alloy Phase Diagrams Materials* (Metal's Park, OH: ASM International)
[26] Paderno Y B, Liashchenko A B, Filippov V B and Dukhnenko A V 2002 *Proc. Int. Conf. on Science for Materials in the Frontier of Centuries: Advantages and Challenges (Kiev) (IPMS NASU)* p 347
[27] Andersen O K 1975 *Phys. Rev.* B **12** 3060–83
[28] Koelling D D and Arbman G O 1975 *J. Phys. F: Met. Phys.* **5** 2041–54
[29] Wimmer E, Krakauer H, Weinert M and Freeman A J 1981 *Phys. Rev.* B **24** 864–75
[30] Jansen H J F and Freeman A J 1984 *Phys. Rev.* B **30** 561–9
[31] Min B I, Oguchi T, Jansen H J F and Freeman A F 1986 *J. Magn. Magn. Mater.* **54–57** 1091–2
[32] Hedin L and Lundqvist B I 1971 *J. Phys. C: Solid State Phys.* **4** 2064–83
[33] Hedin L and Lundqvist S 1972 *J. Physique Coll.* **33** C3 73–81
[34] Jepsen O and Andersen O K 1971 *Solid State Commun.* **9** 1763–7
[35] Lehmann G and Taut M 1972 *Phys. Status Solidi* b **54** 469–77
[36] Herzig P 1985 *Theor. Chim. Acta.* **67** 323–33
[37] Blaha P, Schwarz K and Herzig P 1985 *Phys. Rev. Lett.* **54** 1192–5
[38] Blaha P, Schwarz K and Dederichs P H 1988 *Phys. Rev.* B **37** 2792–6
[39] Massiot D, Fayon F, Capron M, King I, Le Calve S, Alonso B, Durand J-O, Bojuli B, Gan Z H and Hoatson G 2002 *Magn. Reson. Chem.* **40** 70–6
[40] Pyykkö P 1992 *Z. Naturf.* **47**a 189–96
[41] Harima H, Kobayashi N, Takegahara K and Kasuya T 1985 *J. Magn. Magn. Mater.* **52** 367–9
[42] Heinecke M, Winzer K, Noffke J, Kranefeld H, Grieb H, Flachbart K and Paderno Yu B 1995 *Z. Phys.* B **98** 231–7
[43] Shein I R, Okatov S V, Medvedeva N I and Ivanovskii A L 2002 *Preprint* cond-mat/0202015